J Mol Model (2011) 17:2907–2918
DOI 10.1007/s00894-011-0987-6

ORIGINAL PAPER

# Insight into the nature of the interactions of furan and thiophene with hydrogen halides and lithium halides: ab initio and QTAIM studies

**Yanli Zeng · Xiaoyan Li · Xueying Zhang · Shijun Zheng · Lingpeng Meng**

Received: 9 December 2010 / Accepted: 24 January 2011 / Published online: 12 February 2011


**Abstract** The nature of the interactions of furan and thiophene with hydrogen halides and lithium halides has been investigated using ab initio calculations and QTAIM analysis. The concept of molecule formation density difference (MFDD) is introduced to study weak hydrogen bond (HB) and lithium bond (LB) interactions. The results have shown the molecular electrostatic potentials of furan and thiophene, as well as of the hydrogen halides and lithium halides, determine the geometries of the complexes. Both the studied HB and LB interactions can be classified as "closed-shell" weak interactions. The topological properties and energy properties at the bond critical points of HB and LB have been shown to be exponentially dependent on intermolecular distances $d$(H-bond) and $d$(Li-bond), which enables interpretation of the strength of the HB and LB interactions in terms of these $\rho$(r) properties. Electron transfer plays a more important role in the formation of HB than in that of LB, while electrostatic interaction in LB is more dominant than that in HB.

**Keywords** Density difference of molecular formation · Hydrogen bond · Lithium bond · QTAIM study

## Introduction

The hydrogen bond (HB) is the most important weak interaction found in nature. It is responsible for the three-dimensional shapes of biopolymers (proteins and nucleic acids) and for the structure of water in both the liquid and solid phases. Life processes extensively use the making and breaking of hydrogen bonds as part of concatenated reactions involving huge numbers of biomolecules. In addition, hydrogen bonding has profound implications for the mode of action of drugs and in molecular packing, recognition, and crystal engineering [1]. The lithium bond (LB) suggested in 1959 by Shigorin [2] is an interaction analogous to HB in view of the fact that lithium is a congener of hydrogen. Theoreticians first considered such possibilities computationally. The 1970s paper by Kollman et al. [3] entitled "The lithium bond" was influential in delineating the analogy with hydrogen bonding. The existence of LB was confirmed experimentally in 1975 by Ault and Pimentel [4]. Although the concept of LB has been accepted and is important in many fields, studies of LB interactions [5–12] are relatively rare compared to those of HB interactions.

The intermolecular interactions between π-electron systems and Lewis acids have attracted increasing attention in recent years [13–16], because such interactions play a key role in certain chemical reactions, particularly those involving aromatic rings [17, 18]. Compared to simple aromatic compounds, heterocyclic aromatic rings can not only act as π-electron systems but can also offer a nonbonding electron pair (n pair) for the formation of intermolecular interactions. So, O-heterocyclic and S-heterocyclic aromatic rings and their derivatives can form different types of weak interactions with other molecules, including hydrogen halides and dihalogens [19–29].

In the studies of Legon and Millen [19, 20], a set of rules for predicting the angular geometry of complexes of the type B−HX has been proposed, in which the Lewis bases B were chosen as prototypes for different categories of

Y. Zeng · X. Li · X. Zhang · S. Zheng · L. Meng (✉)
Institute of Computational Quantum Chemistry, College of Chemistry and Material Science, Hebei Normal University, Shijiazhuang 050016, People's Republic of China
e-mail: menglp@mail.hebtu.edu.cn

electron donor. According to Legon and Millen's rules, the angular geometry of a system containing both n and π pairs, for example, furan or thiophene, is determined by the n pair.

Lesarri et al. [21] observed the rotational spectrum of the ground vibrational state of the hydrogen-bonded dimer furan···HF, from which they deduced a hydrogen-bonded planar complex of $C_{2v}$ symmetry with the HF subunit lying along the $C_2$ axis of the complex. Shea and Kukolich [22] conducted a Fourier-transform microwave spectroscopy study on furan···HCl, from which they concluded that a hydrogen bond is formed between the HCl proton and the lone pair on oxygen. The structure of furan···HCl has been shown to be planar, giving the complex $C_{2v}$ symmetry, with the HCl axis coincident with the internal $C_2$ axis of the furan ring. In furan···HF and furan···HCl, the respective hydrogen bonds are formed at the site of the furan O atom. However, Cole et al. [23] studied the rotational spectrum of the complex formed by furan and HBr, from which they concluded that furan···HBr does not obey Legon and Millen's rules and adopts π-type geometry. Cooke et al. [24, 25] carried out a pulsed-nozzle, Fourier-transform microwave spectroscopy study on thiophene···HF and thiophene···HCl. They concluded that the non-bonding electron pair on S in thiophene is so weakly nucleophilic that thiophene forms a hydrogen bond with HF or HCl via the aromatic π-electron system. The experimental studies of furan···HBr [23], thiophene···HF [24], and thiophene···HCl [25] raise questions concerning the validity of the rules given by Legon and Millen [19, 20]. To the best of our knowledge, there have not hitherto been any experimental studies on the complexes of furan and thiophene with LiX (X=F, Cl, Br). In view of the close parallelism between lithium bonds and hydrogen bonds, it is reasonable to assume that lithium bonds between furan and thiophene and LiX should also exist.

In this work, the HB interactions between furan and thiophene and HX, as well as the LB interactions between furan and thiophene and LiX, have been investigated. Two different types of intermolecular interactions, namely n-type and π-type interactions, have been studied by means of reliable ab initio calculations and quantum theory of "atoms in molecules" (QTAIM) investigations. The aim of this paper is to compare LB interaction with HB interaction, which should help us to obtain a detailed understanding of the nature of these interactions, enrich the knowledge on such weak interactions, and spur further experimental studies of LB.

## Theoretical methods

The equilibrium geometries of the title systems were fully optimized with the aug-cc-pVDZ basis set at the second-order Møller−Plesset (MP2) level using the GAUSSIAN-03 program package [30]. Harmonic frequencies were calculated to confirm the equilibrium geometries that correspond to energy minima. The keyword counterpoise was used for the calculation of corrected interaction energies ($\Delta E$) excluding the inherent basis set superposition error (BSSE) [31]. Natural bond orbital (NBO) analysis [32] was employed to evaluate the atomic charges on the dimers at the same level. The NBO analysis was carried out using the NBO package included in the GAUSSIAN 03 suite of programs.

In recent works [33, 34], the prototypical directional weak interactions, hydrogen bonding and σ-hole bonding (including the special case of halogen bonding) are reviewed in a united picture that depends on the anisotropic nature of the molecular electrostatic potential around the donor atom. Qualitative descriptions of the effects that lead to these anisotropic distributions are given and examples of the importance of σ-hole bonding in crystal engineering and biological systems are discussed. In this paper, molecular electrostatic potentials on the molecular surfaces of molecular electrostatic potentials of furan and thiophene, as well as of hydrogen halides and lithium halides were computed, after geometry optimization, at the MP2/aug-cc-pVDZ level.

Within the QTAIM theory, a bond between two atoms is characterized by a line of maximum electron density (the bond path) that connects the respective nuclei and intersects the zero-flux surface of the electron density gradient field $\nabla\rho(r)$ at a topological (3,−1) point, called the bond critical point (BCP). The most studied topological properties at the BCP are the electron density $\rho_b$, its Laplacian $\nabla^2\rho_b$, and the eigenvalues of the Hessian matrix ($\lambda_1$, $\lambda_2$, and $\lambda_3$), the latter indicating the three main curvatures of $\rho(r)$ at the BCP. If $\rho(r)$ at the BCP has a saddle distribution, two of the eigenvalues have negative values and correspond to curvatures that are perpendicular to the bond path, while the third is positive and represents the curvature of the $\rho(r)$ distribution along the bond path. By convention, the negative curvatures are $\lambda_1$ and $\lambda_2$ ($\lambda_1<\lambda_2<0$), and the positive one is $\lambda_3$. The Laplacian of the electron density $\nabla^2\rho(r)$, which is defined as the sum of the three eigenvalues of the Hessian, $\lambda_1$, $\lambda_2$, and $\lambda_3$, provides information about either the charge concentration ($\nabla^2\rho(r)<0$) or the charge depletion ($\nabla^2\rho(r)>0$) of the electron distribution [35–37].

A detailed analysis of the electron density distribution function was carried out according to QTAIM as proposed by Bader [35–37], using the programs AIM2000 [38] and GTA-2000 [39], the latter of which was developed by the authors and registered at the QCPE (register number QCPE-661). The properties of the electron density calculated at the bond critical points

(BCP) of the hydrogen bonds and lithium bonds under consideration were characterized. In QTAIM studies, the wave functions were calculated at the MP2/6-311++G(d, p) level since the 6-311++G(d, p) basis set has proven to be more reliable than the aug-cc-pVDZ basis set in AIM calculations of hydrogen bonds [40]. The electron density at the BCP, $\rho_b$; its Laplacian, $\nabla^2\rho_b$; the total electron energy density, $H_b$; and its two components (potential electron energy density, $V_b$, and kinetic electron energy density, $G_b$), have been analyzed on the basis of QTAIM theory.

## Results and discussion

### Equilibrium geometries and interaction energy

As examples of furan···HX, thiophene···HX, furan···LiX, and thiophene···LiX (X=F, Cl, Br), the optimized equilibrium geometries of the complexes furan···HCl, thiophene···HCl, furan···LiCl, and thiophene···LiCl are shown in Fig. 1. For furan···HX and furan···LiX, the geometries can be classified as two types: σ-type and π-type. For thiophene···HX and thiophene···LiX, only π-type complexes can be optimized with no imaginary frequencies. Figure 2a and b present the molecular electrostatic potential (MEP) maps of furan and thiophene. The MEP indicates that the negative electrostatic potential (shown in red) on the n-pair becomes noticeably less negative on going from furan to thiophene, while in the π-electron region it apparently becomes more negative on going from furan to thiophene. This result accounts for the fact that both σ-type and π-type equilibrium geometries are found for furan···HX and furan···LiX, while only π-type equilibrium geometries are found for thiophene···HX and thiophene···LiX.

From Tables 1 and 2, for furan···HX(σ), the O(1)-H(7)-X(8) bond angles are all 180°. For furan···LiX(σ), the O(1)-Li(7)-X(8) bond angles are 111.19°, 120.42°, and 122.91°, respectively. Figure 2c and d present the molecular electrostatic potential (MEP) maps of HCl and LiCl. The MEP indicates that the positive electrostatic potential (shown in blue) resides on the tip of the hydrogen atom of the HCl molecule, but on the "neck" of the lithium atom of the LiCl molecule. In the formation of furan···HX(σ), the "tip" of the hydrogen atom is directed toward the negative electrostatic potential on the n-pair of oxygen, so furan···HX(σ) complexes conform to $C_{2v}$ symmetry, with the HX axis coincident with the internal $C_2$ axis of the furan ring. In the formation of furan···LiX(σ), however, the "neck" of the lithium atom is directed toward the negative electrostatic potential on the n-pair of oxygen, and hence furan···LiX(σ) complexes of planar $C_s$ symmetry are formed.

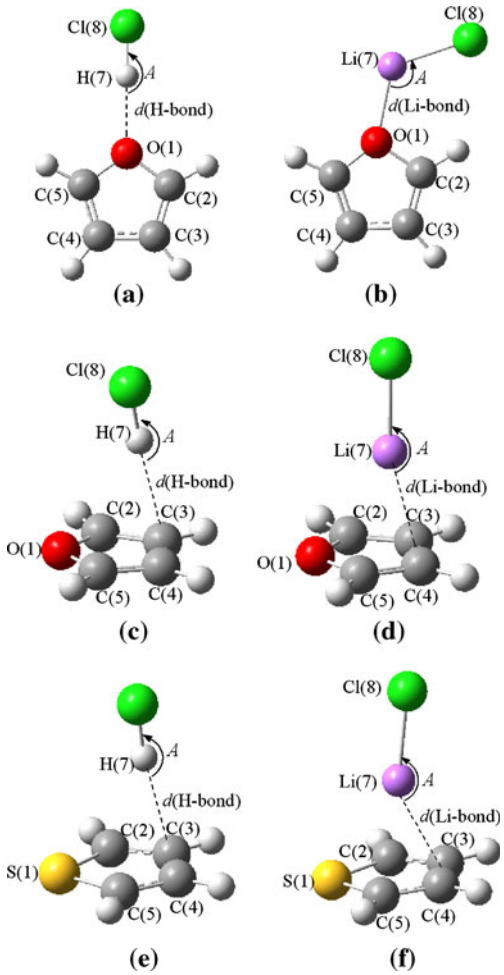


**Fig. 1** Examples of optimized geometries of the hydrogen-bonded and lithium-bonded complexes: furan···HCl(σ) (**a**), furan···LiCl(σ) (**b**), furan···HCl(π) (**c**), and furan···LiCl(π) (**d**), thiophene···HCl(π) (**e**), and thiophene···LiCl(π) (**f**)

The optimized geometries of furan···HX(π) and thiophene···HX(π) conform to $C_1$ symmetry, with the H(7) atom directed toward the C(3) atom. The optimized geometries of furan···LiX(π) and thiophene···LiX(π) conform to $C_s$ symmetry, with the Li(7) atom directed toward the midpoint of the C(3)−C(4) bond. The X(1)-H(7)-C(3) bond angles in furan···HX(π) are larger than the respective X(1)-Li(7)-* angles in furan···LiX(π) and thiophene···LiX(π). These geometries mean that LB has a more "perpendicular" angle than HB.

Tables 1 and 2 lists the interaction energies $\Delta E$ obtained at the MP2/aug-cc-pVDZ level, which have been corrected with BSSE and zero-point vibrational energies (ZPVE). The interaction energies of the lithium-bonded complexes are larger than those of the corresponding hydrogen-bonded complexes, which represents a basic difference between the LB and HB interactions under consideration. The most positive potentials on the hydrogens of HF, HCl and HBr are 74.7, 46.6 and 39.8 kcal·mol$^{-1}$, and those on the

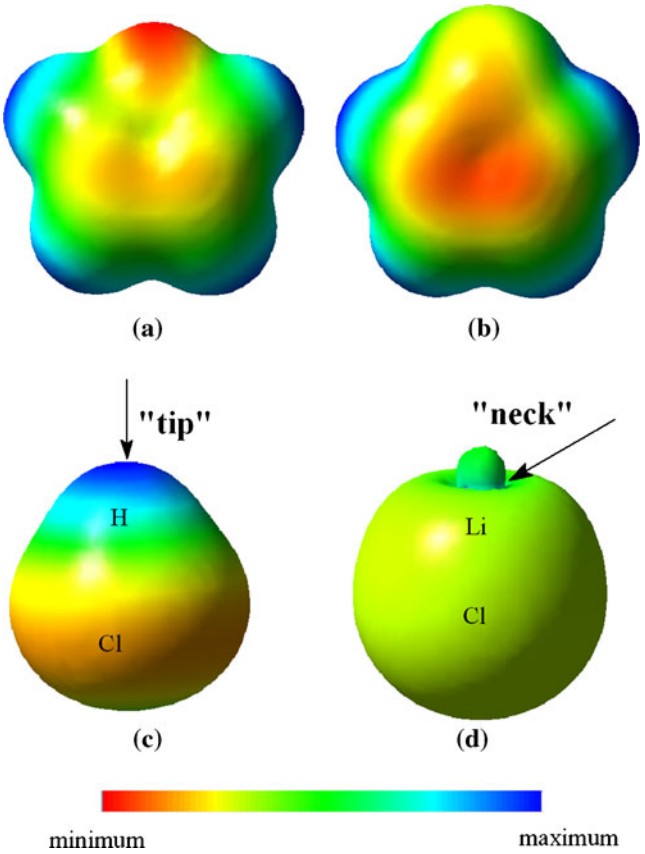


**Fig. 2** Molecular electrostatic potential map of furan (**a**), thiophene (**b**), HCl (**c**) and LiCl (**d**) onto the 0.001 a.u. (electrons/bohr$^3$) contour of the molecule's electronic density

lithiums of LiF, LiCl and LiBr are 1239.3, 1359.2 and 1376.8 kcal·mol$^{-1}$, repectively. The lithium-bonded interactions are stronger than the analogous hydrogen-bonded interactions, following the fact that the most positive potentials on the lithiums are much stronger than those of the hydrogens of the hydrogen halides.

For furan···HX(σ), on going from HF to HCl and HBr, the interaction energies decrease from 14.98 to 11.08 and 9.82 kJ·mol$^{-1}$, while the interaction energies of the corresponding furan···LiX(σ) complexes increase from 48.98 to 54.46 and 55.71 kJ·mol$^{-1}$ on going from LiF to LiCl and LiBr. For both B···HX(π) and B···LiX(π) (B=furan or thiophene), the interaction energies increase in the sequence X=F, Cl, Br.

It is interesting to compare the σ-type complexes with the corresponding π-type complexes. For furan···HF, the σ-type complex is more stable than the corresponding π-type complex. However, for furan···HCl and furan···HBr, the π-type complexes are more stable than the corresponding σ-type complexes. In the case of the lithium-bonded complexes furan···LiX (X=F, Cl, Br), the interaction energies reveal that all of the σ-type complexes are more stable than the corresponding π-type complexes.

## Interaction distances and infrared spectra

In the σ-type complexes, *d*(H-bond) and *d*(Li-bond) denote the distances of the hydrogen or the lithium atom of HX/LiX from the oxygen atom of the furan ring. In furan···HX(π) and thiophene···HX(π), *d*(H-bond) denotes the distance of the hydrogen atom of HX from the C(3) atom of the furan or thiophene ring. In furan···LiX(π) and thiophene···LiX(π), *d* (Li-bond) denotes the distance of the lithium atom of LiX from the midpoint of the C(3) − C(4) bond of furan or thiophene (see Fig. 1). From Table 1, it can be seen that for all of the hydrogen-bonded complexes, *d*(H-bond) increases in the sequence X=F, Cl, Br, which corresponds to the order of decreasing electronegativity of the halogens. However, from Table 2, it can be seen that for all of the lithium-bonded complexes, *d*(Li-bond) decreases in the sequence X=F, Cl, Br. As expected, the H−X and Li−X bonds are lengthened in all of the complexes. The elongation of the H−X bonds varies

**Table 1** Calculated interaction energies, main geometrical parameters, frequencies as well as their changes in the hydrogen-bonded complexes [a]

| | Δ*E* | *d*(H-bond) | Δ*r*(O···H) [b] | Δ*d*(H—X) | *A*(XHY)/*A*(XHC3)[c] | *ν*(H-bond) | Δ*ν*(H—X) |
|---|---|---|---|---|---|---|---|
| furan···HF(σ) | -14.98 | 1.8362 | 0.6538 | 0.0102 | 180.00 | 143.72 | -230.45 |
| furan···HCl(σ) | -11.08 | 2.0120 | 0.4780 | 0.0090 | 180.00 | 90.42 | -121.44 |
| furan···HBr(σ) | -9.82 | 2.0836 | 0.4064 | 0.0074 | 180.00 | 65.82 | -85.32 |
| furan···HF(π) | -11.85 | 2.2609 | | 0.0080 | 169.75 | 119.73 | -187.04 |
| furan···HCl(π) | -12.41 | 2.4156 | | 0.0091 | 176.29 | 89.46 | -124.39 |
| furan···HBr(π) | -12.57 | 2.4714 | | 0.0085 | 176.27 | 72.14 | -100.01 |
| thiophene···HF(π) | -12.73 | 2.3135 | | 0.0078 | 164.10 | 115.16 | -179.56 |
| thiophene···HCl(π) | -14.37 | 2.4166 | | 0.0091 | 171.58 | 87.80 | -121.34 |
| thiophene···HBr(π) | -14.81 | 2.4617 | | 0.0086 | 171.89 | 70.94 | -98.16 |

[a] Interaction energies in kJ·mol$^{-1}$, bond lengths in angstrom, bond angles in degree, and frequencies in cm$^{-1}$

[b] Δ*r*(O···H) denotes the decreases of bond distance *d*(H-bond) in the complexes compared to the sum of van der Waals radii of O atom and H atom

[c] Y = O and S

**Table 2** Calculated interaction energies, main geometrical parameters, frequencies as well as their changes in the lithium-bonded complexes [a]

| | $\Delta E$ | $d$(Li-bond) | $\Delta r$(O···Li) [b] | $\Delta d$(Li–X) | $A$(XLiY)/$A$(XLi*)[c] | $\nu$(Li-bond) | $\Delta\nu$(Li–X) |
|---|---|---|---|---|---|---|---|
| furan···LiF(σ) | -48.98 | 2.0264 | 1.1936 | 0.0315 | 111.19 | 320.81 | -63.47 |
| furan···LiCl(σ) | -54.56 | 1.9965 | 1.2235 | 0.0356 | 120.42 | 315.74 | -18.50 |
| furan···LiBr(σ) | -55.71 | 1.9913 | 1.2287 | 0.0373 | 122.91 | 304.99 | 1.00 |
| furan···LiF(π) | -36.01 | 2.4350 | | 0.0176 | 166.56 | 153.32 | -21.95 |
| furan···LiCl(π) | -45.15 | 2.3812 | | 0.0239 | 165.47 | 142.26 | 6.78 |
| furan···LiBr(π) | -47.31 | 2.3744 | | 0.0263 | 166.56 | 123.50 | 22.27 |
| thiophene···LiF(π) | -40.18 | 2.4592 | | 0.0208 | 151.04 | 158.21 | -30.86 |
| thiophene···LiCl(π) | -51.08 | 2.3952 | | 0.0293 | 150.32 | 161.28 | -2.81 |
| thiophene···LiBr(π) | -53.72 | 2.3842 | | 0.0318 | 150.29 | 158.43 | 15.57 |

[a] Interaction energies in kJ·mol$^{-1}$, bond lengths in angstrom, bond angles in degree, and frequencies in cm$^{-1}$

[b] $\Delta r$(O···Li) denote the decreases of bond distance $d$(Li-bond) in the complexes compared to the sum of van der Waals radii of O atom and Li atom

[c] Y=O and S, * denotes the midpoint of C3-C4 bond

from 0.0074 to 0.0102 Å, and the elongation of the Li − X bonds varies from 0.0176 to 0.0373 Å. The elongation of the Li−X bonds is larger than that of the H − X bonds. Except for furan···HF(π) and thiophene···HF(π), the H − X bond elongation decreases in the following order: B···HF>B···HCl>B···HBr (B=furan and thiophene). For the lithium-bonded complexes, however, the Li−X bond elongation increases in the following order: B···LiF<B···LiCl<B···LiBr (B=furan and thiophene). According to the above analyses, it is clear that the H−X and Li−X bond elongations are consistent with the intermolecular distances. The shorter $d$(H-bond) and $d$(Li-bond), the larger the variations $\Delta d$(H−X) and $\Delta d$(Li−X).

In Tables 1 and 2, $\Delta r$(O···H) and $\Delta r$(O···Li) represent the decrease of bond distance $d$(H-bond) and $d$(Li-bond) in the complexes compared to the sum of van der Waals radii of O atom and H, Li atom. This indicates that weak interactions indeed exist in the complexes. Moverover, $\Delta r$(O···H) and $\Delta r$(O···Li) show the lithium-bonded complexes have much lower ratios than the hydrogen-bonded ones, following the fact that the most positive potentials on the lithiums are much stronger than those of the hydrogens of the hydrogen halides.

The vibrational frequencies of the hydrogen bonds, $\nu$(H-bond), decrease in the order B···HF>B···HCl>B···HBr (B=furan and thiophene). The vibrational frequencies of the lithium bonds, $\nu$(Li-bond), also decrease in the order B···LiF>B···LiCl>B···LiBr. The lithium bond frequency $\nu$(Li-bond) is larger than the corresponding $\nu$(H-bond) for all of the complexes. In accordance with the H−X bond elongation in the formation of hydrogen-bonded complexes, the H−X stretching vibrations shift to lower frequencies. The degree of red-shift of $\Delta\nu$(H−X) is consistent with the $\nu$(H-bond). The larger $\nu$(H-bond), the larger the variation $\Delta\nu$(H−X). For the furan···LiF(σ), furan···LiCl(σ), furan···LiF(π), thiophene···LiF(π), and thiophene···LiCl(π) complexes, the Li−X stretching vibration moves to lower frequency upon complex formation, whereas for the furan···LiBr(σ), furan···LiCl(π), furan···LiBr (π), and thiophene···LiBr(π) complexes the Li−X stretching vibration shifts to higher frequency. These are abnormal blue shifts of the Li−X stretching frequency, which are inconsistent with the Li−X bond elongations. Similar observations have been made for some other lithium-bonded complexes [41–45]. Li et al. [40] tested the reliability of the abnormal blue shift by five different methods, including QCISD/aug-cc-pVDZ. In all cases, the abnormal blue shift was corroborated. Feng et al. [41] postulated that a possible reason for this inconsistency may be coupling between the Li−X vibration and the vibrations of other bonds. We think that the origin of such elongated but blue-shifted lithium bonds still requires further investigation.

## QTAIM analyses

In recent years, the QTAIM theory [35–37] has been widely applied to study the electronic structures of molecules, chemical bonds, chemical reactions, and systems involving weak interactions [46–57]. The topological characterization of conventional lithium bonding has been studied in several LiF complexes [11]. The results show that the electron density $\rho_b$ at lithium bond critical points (BCPs) is about half of that in the hydrogen-bonded analogues, suggesting a dominant role of electrostatic interaction rather than charge transfer in the lithium-bonded complexes.

### *A. Molecular graphs*

The molecular graphs of furan···HCl, thiophene···HCl, furan···LiCl, and thiophene···LiCl are shown in Fig. 3. For furan···HCl(σ), there is an interaction line between the H atom of the HCl molecule and the O atom of the furan molecule. For furan···LiCl(σ), except for the lithium bond

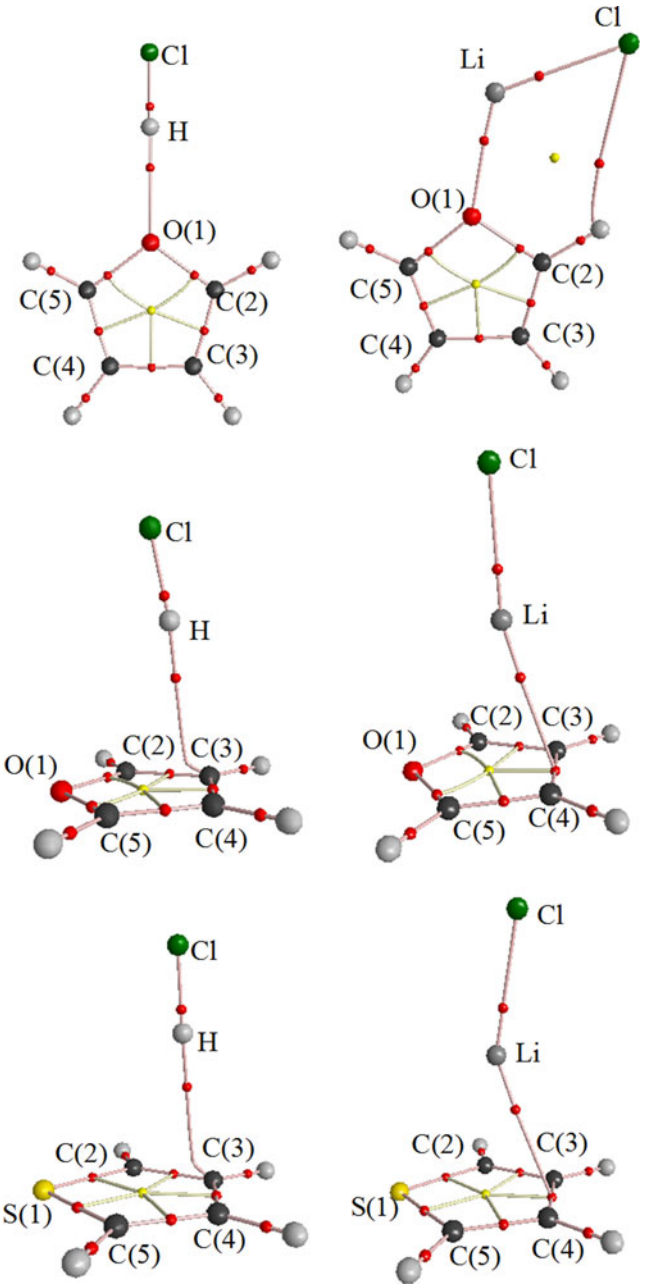


**Fig. 3** Examples of molecular graphs of the hydrogen-bonded and lithium-bonded complexes

between the Li atom of the LiCl molecule and the O atom of the furan molecule, the five-membered ring structure indicates the existence of secondary interactions. This is consistent with the interaction energies of σ-type lithium-bonded complexes being larger than those of σ-type hydrogen-bonded complexes. For furan···HCl(π) and thiophene···HCl(π), there is an interaction line between the H atom of the HCl molecule and the C(3) atom of the furan or thiophene molecule. For furan···LiCl(π) and thiophene···LiCl(π), there is an interaction line between the Li atom and the BCP of the C(3) − C(4) bond of molecule B, which indicates that both the C(3) and C(4) atoms interact with the Li atom.

### *B. Topological properties at the BCP*

According to the topological analysis of electronic density distribution in the AIM theory, $\rho_b$ is used to describe the strength of a bond. In general, the larger the value of $\rho_b$, the stronger the bond [33]. From Table 3, it is clear that for both σ-type and π-type hydrogen-bonded complexes, $\rho_b$ decreases in the order B···HF>B···HCl>B···HBr (B=furan or thiophene). This means that the B···HF bond is the strongest, the B···HCl bond is weaker, and the B···HBr bond is the weakest. However, from Table 4, for both σ-type and π-type lithium-bonded complexes, $\rho_b$ increases in the order B···LiF<B···LiCl<B···LiBr (B=furan or thiophene), indicating that the B···LiF bond is the weakest, the B···LiCl bond is stronger, and the B···LiBr bond is the strongest. From Tables 3 and 4, the most positive potentials on the hydrogens of HF, HCl and HBr decrease as the halogen increases in size, while those on the lithiums of LiF, LiCl and LiBr increase as the halogen increases in size. This follows the trends in their respective bond strength.

Despite the much larger interaction energies of LB compared to HB, the electron density at the BCP in LB is nearly the same as that at the BCP in HB, suggesting a dominant role of electrostatic interaction rather than charge transfer in the LB complexes. The larger interaction energies of LB complexes are due to electrostatic interactions, as proposed by Berski and Latajka on the basis of an ELF analysis [58].

When σ-type and π-type hydrogen-bonded complexes are considered together, the topological properties at the BCP (the electron density $\rho_b$, its Laplacian $\nabla^2\rho_b$, and the eigenvalue $\lambda_3$ of the Hessian matrix) of HB are seen to be exponentially related to the intermolecular distance $d$(H-bond) for B···HX (B=furan or thiophene; X=F, Cl, Br). Similar relationships were also found for B···LiX lithium-bonded systems, see Fig. 4. This exponential relationship between $\rho_b$ of HB and $d$ (H-bond) is similar to that delineated in Tang's study on hydrogen-bonded complexes [59].

$$\rho_b(\mathrm{HB}) = 3.40516 \times \exp[-d(\mathrm{H-bond})/0.34039] + 0.00979 \quad R^2 = 0.9975$$

$$\rho_b(\mathrm{LB}) = 14.05481 \times \exp[-d(\mathrm{Li-bond})/0.29181] + 0.00703 \quad R^2 = 0.9927$$

$$\nabla^2\rho_b(\mathrm{HB}) = 18.28893 \times \exp[-d(\mathrm{H-bond})/0.35745] + 0.01231 \quad R^2 = 0.9956$$

$$\nabla^2\rho_b(\mathrm{LB}) = 1017.35436 \times \exp[-d(\mathrm{Li-bond})/0.22359] + 0.03983 \quad R^2 = 0.9578$$

$$\lambda_3(\mathrm{HB}) = 60.10066 \times \exp[-d(\mathrm{H-bond})/0.31284] + 0.02622 \quad R^2 = 0.9985$$

$$\lambda_3(\mathrm{LB}) = 10839.9656 \times \exp[-d(\mathrm{Li-bond})/0.18373] + 0.04693 \quad R^2 = 0.9578$$

**Table 3** Topological and energy properties of hydrogen bond critical point in the hydrogen-bonded complexes

| | $V_{S,max}$ [a] | $\rho_b$ [b] | $\nabla^2\rho_b$ [b] | $H_b$ [b] | $-G_b/V_b$ |
|---|---|---|---|---|---|
| furan···HF(σ) | 74.7 (*H–F) | 0.0251 | 0.1202 | 0.0039 | 1.1734 |
| furan···HCl(σ) | 46.6 (*H–Cl) | 0.0193 | 0.0787 | 0.0031 | 1.2307 |
| furan···HBr(σ) | 39.8 (*H–Br) | 0.0172 | 0.0661 | 0.0027 | 1.2392 |
| furan···HF(π) | 74.7 (*H–F) | 0.0144 | 0.0453 | 0.0023 | 1.3536 |
| furan···HCl(π) | 46.6 (*H–Cl) | 0.0129 | 0.0345 | 0.0015 | 1.2693 |
| furan···HBr(π) | 39.8 (*H–Br) | 0.0122 | 0.0317 | 0.0013 | 1.2492 |
| thiophene···HF(π) | 74.7 (*H–F) | 0.0136 | 0.0436 | 0.0025 | 1.4219 |
| thiophene···HCl(π) | 46.6 (*H–Cl) | 0.0124 | 0.0340 | 0.0015 | 1.2690 |
| thiophene···HBr(π) | 39.8 (*H–Br) | 0.0119 | 0.0265 | 0.0013 | 1.2438 |

[a] $V_{S,max}$ values in kcal mol$^{-1}$ ;
[b] Topological and energy properties in a.u

Thus, for both the HB and LB interactions under consideration, the topological properties $\rho_b$, $\nabla^2\rho_b$, and the curvature $\lambda_3$ may be well represented by an exponential function of the intermolecular distance.

### *C. Energy properties at the BCP*

Topological properties at the BCP of the HB and LB, such as the Laplacian of the electron density $\nabla^2\rho_b$, the kinetic electron energy density ($G_b$), the potential electron energy density ($V_b$), the electron energy density $H_b$ (the sum of $G_b$ and $V_b$), and $-G_b/V_b$, are listed in Tables 3 and 4.

The values of $\nabla^2\rho_b$ and $H_b$ derived from the Bader theory indicate the nature of the interaction. A negative value of the Laplacian of electron density at the BCP indicates that there is a shared interaction as in a covalent bond. A positive value of $\nabla^2\rho_b$ indicates the interaction of closed-shell systems, that is, ionic interactions, van der Waals forces, or hydrogen bonding [35]. It has also been claimed that if $\nabla^2\rho_b$ is positive but $H_b$ is negative, then the interaction is partly covalent in nature [60, 61]. The kinetic electron energy density $G_b$ is positive, the potential electron energy density $V_b$ is negative, and the balance between these two values determines the nature of the interaction. Hence, $-G_b/V_b$ may indicate the regions corresponding to covalent or noncovalent interactions. If this ratio is greater than 1, then the interaction is noncovalent. If the ratio is between 0.5 and 1, the interaction is partly covalent in nature, and when $-G_b/V_b$ is less than 0.5, the interaction is a shared covalent one. From Tables 3 and 4, it can be seen that for all of the hydrogen-bonded and lithium-bonded systems considered here, the $\nabla^2\rho_b$ values are positive, the $H_c$ values are positive, and the $-G_b/V_b$ values are greater than 1. Hence, the HB and LB interactions display all of the hallmarks of "closed-shell" interactions, indicating that the charge density is concentrated toward the atomic basins rather than accumulated at the critical point.

Rozas et al. [62] suggested that both the Laplacian $\nabla^2\rho_b$ and the energy density $H_b$ should be used as criteria to characterize hydrogen bonding. They found that weak hydrogen bonds are characterized by $\nabla^2\rho_b>0$ and $H_b>0$, medium hydrogen bonds by $\nabla^2\rho_b>0$ and $H_b<0$, and strong hydrogen bonds by $\nabla^2\rho_b<0$ and $H_b<0$. From Tables 3 and 4, it can be seen that for all of the studied hydrogen-bonded complexes $\nabla^2\rho_b>0$ and $H_b>0$, which indicates that the HB interactions in B···HX are weak hydrogen bonds. For the studied lithium-bonded complexes, $\nabla^2\rho_b>0$ and $H_b>0$, from which it can be concluded that the LB interactions in B···LiX are also weak.

**Table 4** Topological and energy properties of lithium bond critical point in the lithium-bonded complexes

| | $V_{S,max}$ [a] | $\rho_b$ [b] | $\nabla^2\rho_b$ [b] | $H_b$ [b] | $-G_b/V_b$ |
|---|---|---|---|---|---|
| furan···LiF(σ) | 1239.3 (*Li–F) | 0.0200 | 0.1566 | 0.0079 | 1.3394 |
| furan···LiCl(σ) | 1359.2 (*Li–Cl) | 0.0222 | 0.1751 | 0.0088 | 1.3357 |
| furan···LiBr(σ) | 1376.8 (*Li–Br) | 0.0226 | 0.1784 | 0.0089 | 1.3350 |
| furan···LiF(π) | 1239.3 (*Li–F) | 0.0102 | 0.0510 | 0.0021 | 1.2502 |
| furan···LiCl(π) | 1359.2 (*Li–Cl) | 0.0115 | 0.0588 | 0.0024 | 1.2368 |
| furan···LiBr(π) | 1376.8 (*Li–Br) | 0.0118 | 0.0600 | 0.0024 | 1.2289 |
| thiophene···LiF(π) | 1239.3 (*Li–F) | 0.0093 | 0.0495 | 0.0021 | 1.2626 |
| thiophene···LiCl(π) | 1359.2 (*Li–Cl) | 0.0108 | 0.0920 | 0.0024 | 1.2521 |
| thiophene···LiBr(π) | 1376.8 (*Li–Br) | 0.0111 | 0.0600 | 0.0025 | 1.2468 |

[a] $V_{S,max}$ values in kcal mol$^{-1}$ ;
[b] Topological and energy properties in a.u.

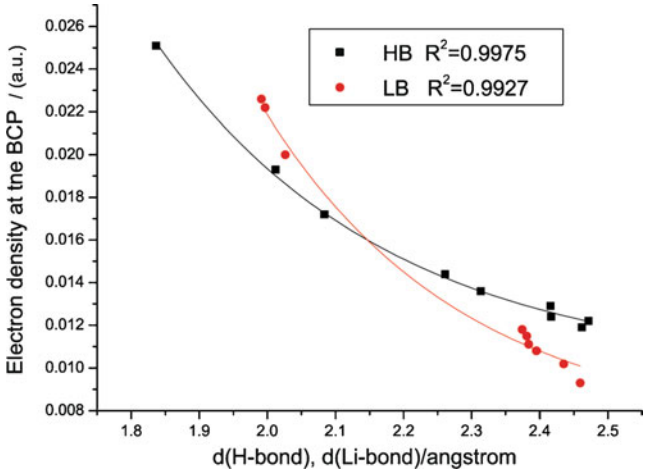


**Fig. 4** Exponential dependencies between electron density $\rho_b$ at the BCP and intermolecular distance d(H-bond) and d(Li-bond)

The $\nabla^2\rho_b$ and $G_b$ values of LB are larger than those of HB, while the $V_b$ values of LB are smaller than those of HB, which indicates that the electrostatic interactions in LB are more dominant than those in HB.

From Table 3, it can be seen that for HB the values of $\nabla^2\rho_b$, $G_b$, and $H_b$ decrease while $V_b$ increases in the series X=F, Cl, Br. However, the opposite trends are observed for LB (Table 4). These findings indicate that in the series X=F, Cl, Br the electrostatic interactions become weaker for HB interactions but become stronger for LB interactions.

Comparing the σ-type and π-type hydrogen-bonded complexes, the values of $G_b$ and $V_b$ of HB are seen to be exponentially dependent on the intermolecular distance $d$ (H-bond); similar features have also been found for the B···LiX systems (Fig. 5a). The fitted curves can be represented as follows.

$$G_b(\mathrm{HB}) = 13.25153 \times \exp[-d(\mathrm{H-bond})/0.28746] + 0.00414 \quad R^2 = 0.9991$$

$$V_b(\mathrm{HB}) = -27.61598 \times \exp[-d(\mathrm{H-bond})/0.25211] - 0.00360 \quad R^2 = 0.9957$$

$$G_b(\mathrm{LB}) = 673.48376 \times \exp[-d(\mathrm{Li-bond})/0.19694] + 0.00833 \quad R^2 = 0.9987$$

$$V_b(\mathrm{LB}) = -248.97475 \times \exp[-d(\mathrm{Li-bond})/0.21123] - 0.00655 \quad R^2 = 0.9977$$

In addition to the exponential dependences of $G_b$, $V_b$, and the intermolecular distances, excellent linear relationships between $V$ and the sum of the perpendicular curvatures, $\lambda_1+\lambda_2$, and between $G$ and the curvature along the bond path direction, $\lambda_3$, have been found for B···HX. Similar linear relationships were also found for B···LiX systems (Fig. 5b).

$$G_b(\mathrm{HB}) = -3.48461 \times 10^{-5} + 0.13391 \times \lambda_3 \quad R^2 = 0.9992$$

$$V_b(\mathrm{HB}) = 2.66398 \times 10^{-4} + 0.30028 \times (\lambda_1 + \lambda_2) \quad R^2 = 0.9960$$

$$G_b(\mathrm{LB}) = 0.00291 + 0.12651 \times \lambda_3 \quad R^2 = 0.9996$$

$$V_b(\mathrm{LB}) = -0.00835 + 0.21056 \times (\lambda_1 + \lambda_2) \quad R^2 = 0.9406$$

The topological and energy dependences on intermolecular distance observed for HB and LB "closed-shell" weak interactions enabled interpretation of the strength of the HB and LB interactions in terms of these $\rho(r)$ properties.

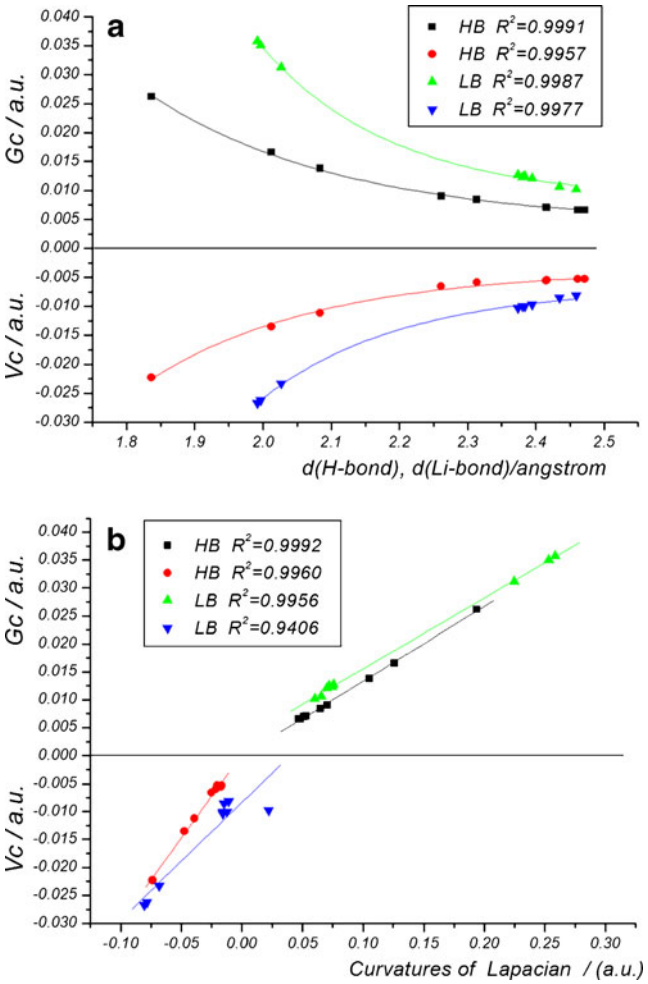


**Fig. 5** Exponential relationships between local energy densities ($G_b$ and $V_b$) at the BCP and intermolecular distance d(H-bond) and d(Li-bond), as well as linear relationships between local energy densities ($G_b$ and $V_b$) and electron density curvatures ($G_b$ with $\lambda_3$ and $V_b$ with $\lambda_1+\lambda_2$)

Upon bond formation, a maximum distribution of $\rho$(r) is created along the bond path. The curvatures of the electron distribution in the perpendicular plane at any point of the bond path, and in particular at the BCP, increase with increasing concentration of $\rho$(r). Along the bond path, $\rho$(r) decreases from the nuclei toward the BCP, where it has a local minimum, and the curvature along this direction increases with charge depletion. The increase of the negative magnitude $\lambda_1 + \lambda_2$ is accompanied by an increase of the positive amplitude, $\lambda_3$, indicating that a sharper electron concentration in the plane where $\rho$(r) reaches a maximum is necessarily followed by greater $\rho$(r) depletion along the direction of the bond path [37]. Thus, at the BCP, $V_b$ and $G_b$ are related to the charge concentration of $\rho$(r) in the plane perpendicular to the bond path and to its charge depletion along the path direction, respectively. The linear relationships observed for both HB and LB interactions between the local energy densities and the topological curvatures reflect this situation.

*D. Density difference of molecule formation (MFDD)*

For a super-molecule A-B, the MFDD is defined as:

$$\rho_d(r) = \rho_{complex}(r) - (\rho_{molA}(r) + \rho_{molB}(r)).$$

Explicit images of the interactions between molecules A (furan or thiophene) and B (HCl or LiCl) are plotted on the basis of the distribution of function $\rho_d$(r), as shown in Fig. 6. The MFDD graphs clearly show the formation processes of HB and LB.

For furan···HCl(σ) and furan···LiCl(σ), the electron density of the O atom of furan decreases in the formation of HB and LB. Concomitantly, electron density increases in the region between the H/Li atom of HX/LiX and the O atom of furan, and the increased region between the H and O atoms in furan···HCl(σ) is larger than that between the Li and O atoms in furan···LiCl(σ). For furan···HCl(π) and furan···LiCl(π), the electron density on furan decreases and it increases in the region between the H/Li atom of HX/LiX and the furan; the increased region in furan···HCl(π) is larger than that in furan···LiCl(π). For thiophene···HCl(π) and thiophene···LiCl(π), the electron density on thiophene decreases and it increases in the region between the H/Li atom of HX/LiX and the thiophene; the increased region in thiophene···HCl(π) is also larger than that in thiophene···LiCl(π). Figure 6 indicates that electron transfer occurs from the O atom of furan to the H/Li atom in the formation of σ-type HB and LB, and from the furan or thiophene ring to the H/Li atom in the formation of π-type HB and LB.

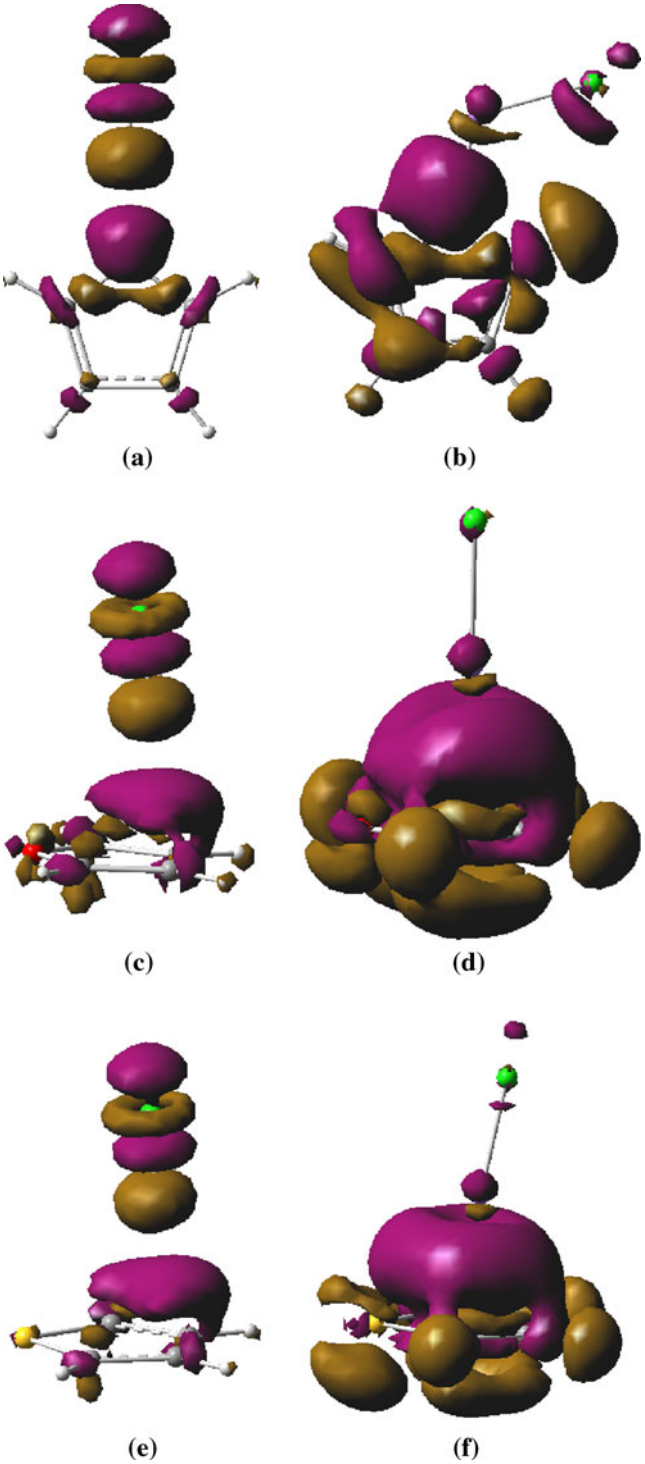


**Fig. 6** Molecular formation density difference map of furan···HCl(σ) (**a**), furan···LiCl(σ) (**b**), furan···HCl(π) (**c**), furan···LiCl(π) (**d**), thiophene···HCl(π) (**e**), and thiophene···LiCl(π) (**f**) onto the 0.0008 a.u. (in brown, gain electron) and -0.0008 a.u. (in purple, loss electron) contour of the molecule's electronic density

From the above discussions, the regions of increased electron density between furan or thiophene and HCl are larger than those between furan or thiophene and LiCl. Moreover, in the hydrogen-bonded complexes, regions of

increased electron density exist not only between the H atom and furan or thiophene, but also around the Cl atom. For the lithium-bonded complexes, however, the increased region is only between the Li atom and furan or thiophene. The MFDD indicates that electron transfer plays a more important role in the formation of the hydrogen-bonded complexes than in that of the lithium-bonded complexes. The differences in the regions of increased electron density of hydrogen-bonded and lithium-bonded complexes are consistent with the charge transfers, with the X atom being the main electron acceptor in charge transfer from B to HX and the Li atom being the main electron acceptor in charge transfer from B to LiX (B=furan or thiophene).

### NBO analysis

For a better understanding of the HB and LB, NBO analysis was carried out at the HF/aug-cc-pVDZ level of theory using the MP2/aug-cc-pVDZ geometry. The occupancy ($\delta$) of frontier molecular orbitals involving charge transfer (CT) between subsystems, the second-order perturbation energy lowering ($\Delta^2E$) due to the interaction of donor and acceptor orbitals, and the quantity of charge transferred from the donor to the acceptor $q_{CT}$, as provided by NBO analysis, are collected in Tables 5 and 6.

For furan···HX(σ), electron transfer occurs from the lone pair orbital of the O atom to the anti-bonding orbital of HX (X=F, Cl, Br). For furan···HX(π) and thiophene···HX(π), it occurs from the C2 − C3 π-bond pair to the anti-bonding orbital of HX. For furan···LiX(σ), it occurs from the lone pair orbital of the O atom to the Li anti-bonding lone pair orbital of the electron acceptor LiX. For furan···LiX(π) and thiophene···LiX(π), it occurs from the C2 − C3 and C4−C5 π-bond pairs to the Li anti-bonding lone pair orbitals. These conclusions are consistent with the topological molecular graphs (Fig. 3), which show that an interaction line exists between the Li atom and the BCP of the C(3) − C(4) bond of furan or thiophene for B···LiX(π), and between the H atom and the C(3) atom of furan or thiophene for B···HX (π). These findings are in good agreement with the fact that the interaction energies of lithium-bonded complexes are much larger than those of hydrogen-bonded complexes.

The $q_{CT}$ and $\Delta^2E$ values of the σ-complexes are larger than those of the π-complexes. Moreover, $q_{CT}$ and $\Delta^2E$ decrease in the order HF > HCl > HBr, but increase in the order LiF < LiCl < LiBr. These orders exactly match those of electron density, $\rho_b$, of HB and LB. We found that the higher the electron density ($\rho_b$), the more charge was transferred from the donor to the acceptor ($q_{CT}$), and the greater the second-order perturbation energy lowering ($\Delta^2E$). Good linear relationships were found between the electron density, $\rho_b$, of HB and LB and charge transfer $q_{CT}$ (Fig. 7a), with linear correlation coefficients of 0.9939 and 0.9851 for B···HX and B···LiX, respectively. Figure 7b shows the linear relationships between $\rho_b$ of HB and LB and the second-order perturbation energy lowering $\Delta^2E$. The linear correlation coefficients are 0.9717 and 0.9416 for the B···HX and B···LiX series, respectively.

Comparing the $q_{CT}$ and $\Delta^2E$ values for LB with those for HB, one can see that the $q_{CT}$ values for HB are a little larger than those for LB, and the $\Delta^2E$ values for HB are a little larger than those for LB. These observations indicate that charge transfer plays a more important role in hydrogen-bonded complexes than in lithium-bonded complexes, which is in good agreement with the results concerning MFDD analysis.

## Conclusions

(1) Furan···HF favors σ-type HB interaction, whereas furan···HCl and furan···HBr favor π-type HB interactions. Furan···LiX (X=F, Cl, Br) favor σ-type LB interactions. Only π-type geometries for thiophene···HX and furan···LiX (X = F, Cl, Br) can be optimized with no imaginary frequencies. The molecular electrostatic potentials of furan and thiophene, as well as of hydrogen halides and lithium halides, determine the geometries of the complexes.

**Table 5** Natural bond orbital analysis for the hydrogen-bonded complexes. ($\Delta^2$E in kcal mol$^{-1}$, $q_{CT}$ in a.u.)

| Geometry | Donor NBOs | $\delta$ | Acceptor NBOs | $\delta$ | $q_{CT}$ | $\Delta^2E$ |
|---|---|---|---|---|---|---|
| furan···HF(σ) | O lone pair | 1.9686 | H-F anti-bond | 0.0128 | 0.104 | 8.62 |
| furan···HCl(σ) | O lone pair | 1.9681 | H-Cl anti-bond | 0.0118 | 0.081 | 6.67 |
| furan···HBr(σ) | O lone pair | 1.9680 | H-Br anti-bond | 0.0120 | 0.075 | 6.12 |
| furan···HF(π) | C2-C3 π-bond pair | 1.8937 | H-F anti-bond | 0.0093 | 0.064 | 4.53 |
| furan···HCl(π) | C2-C3 π-bond pair | 1.8881 | H-Cl anti-bond | 0.0114 | 0.054 | 4.52 |
| furan···HBr(π) | C2-C3 π-bond pair | 1.8863 | H-Br anti-bond | 0.0128 | 0.052 | 4.63 |
| thiophene···HF(π) | C2-C3 π-bond pair | 1.8895 | H-F anti-bond | 0.0074 | 0.059 | 3.83 |
| thiophene···HCl(π) | C2-C3 π-bond pair | 1.8833 | H-Cl anti-bond | 0.0094 | 0.050 | 3.77 |
| thiophene···HBr(π) | C2-C3 π-bond pair | 1.8818 | H-Br anti-bond | 0.0108 | 0.048 | 3.93 |

**Table 6** Natural bond orbital analysis for the lithium-bonded complexes. ($\Delta^2$E in kcal mol$^{-1}$, $q_{CT}$ in a.u.)

| Geometry | Donor NBOs | $\delta$ | Acceptor NBOs | $\delta$ | $q_{CT}$ | $\Delta^2E$ |
|---|---|---|---|---|---|---|
| furan···LiF(σ) | O lone pair | 1.9738 | Li anti-lone pair | 0.0208 | 0.069 | 5.01 |
| furan···LiCl(σ) | O lone pair | 1.9694 | Li anti-lone pair | 0.0584 | 0.082 | 6.90 |
| furan···LiBr(σ) | O lone pair | 1.9683 | Li anti-lone pair | 0.0730 | 0.087 | 7.83 |
| furan···LiF(π) | C2-C3 π-bond pair | 1.8895 | Li anti-lone pair | 0.0261 | 0.039 | 2.32 |
| | C4-C5 π-bond pair | 1.8895 | | | 0.039 | 2.32 |
| furan···LiCl(π) | C2-C3 π-bond pair | 1.8863 | Li anti-lone pair | 0.0779 | 0.048 | 3.57 |
| | C4-C5 π-bond pair | | | | 0.048 | 3.57 |
| furan···LiBr(π) | C2-C3 π-bond pair | 1.8843 | Li anti-lone pair | 0.0981 | 0.049 | 4.07 |
| | C4-C5 π-bond pair | 1.8843 | | | 0.049 | 4.07 |
| thiophene···LiF(π) | C2-C3 π-bond pair | 1.8828 | Li anti-lone pair | 0.0293 | 0.035 | 1.96 |
| | C4-C5 π-bond pair | 1.8828 | | | 0.035 | 1.96 |
| thiophene···LiCl(π) | C2-C3 π-bond pair | 1.8786 | Li anti-lone pair | 0.0846 | 0.046 | 3.30 |
| | C4-C5 π-bond pair | 1.8786 | | | 0.046 | 3.30 |
| thiophene···LiBr(π) | C2-C3 π-bond pair | 1.8793 | Li anti-lone pair | 0.1054 | 0.047 | 3.75 |
| | C4-C5 π-bond pair | 1.8793 | | | 0.047 | 3.75 |

(2) Similarity between HB and LB:

(i) The studied HB and LB interactions can be classified as "closed-shell" weak interactions.

(ii) For the studied HB and LB interactions, we found that the topological properties at the BCP (the electron density $\rho_b$, its Laplacian $\nabla^2\rho_b$, and the eigenvalue $\lambda_3$ of the Hessian matrix), as well as the energy properties ($G_b$ and $V_b$) of HB and LB, were exponentially dependent on the intermolecular distances $d$(H-bond) and $d$(Li-bond), which enabled interpretation of the strength of the HB and LB interactions in terms of these $\rho$(r) properties.

(iii) Excellent linear relationships between $V$ and the sum of the perpendicular curvatures, $\lambda_1 + \lambda_2$, and between $G$ and the curvature along the bond path direction, $\lambda_3$, have been found for both HB and LB.

(iv) Charge transfers were observed from B to HX and LiX in the hydrogen-bonded and lithium-bonded complexes by analysis of the MFDD and NBO.

(v) Good linear relationships exist between the electron density, $\rho_b$, of HB and LB and charge transfer $q_{CT}$, as well as the second-order perturbation energy lowering ($\Delta^2E$). We found that the higher the electron density ($\rho_b$), the more charge is transferred from the donor to the acceptor ($q_{CT}$), and the larger the second-order perturbation energy lowering ($\Delta^2E$).

(3) Differences between HB and LB:

(i) The interaction energies of the studied lithium-bonded complexes are larger than those of the corresponding hydrogen-bonded complexes, representing a basic difference between LB and HB.

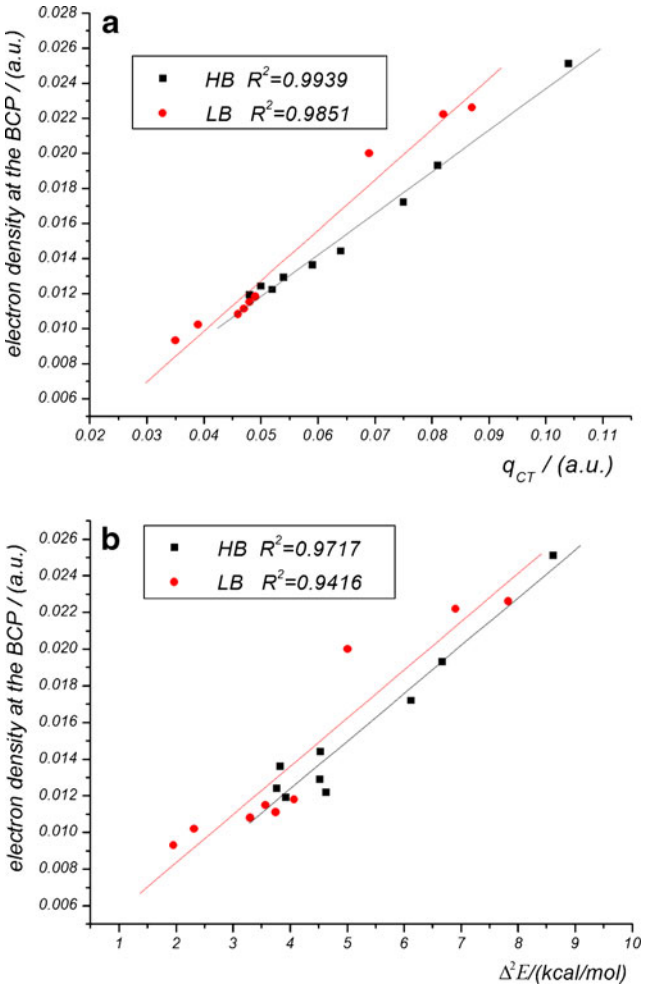


**Fig. 7** Linear relationships between electron density $\rho_b$ of HB and LB and charge transfer $q_{CT}$, as well as linear relationships between $\rho_b$ and second-order perturbation energy lowering $\Delta^2$E

(ii) The bond strength of HB conforms to the order B···HF>B···HCl>B···HBr, while the bond strength of LB conforms to the order B···LiF<B···LiCl<B···LiBr.

(iii) Electron transfer plays a more important role in the formation of HB than in the formation of LB; the electrostatic interaction in LB is more dominant than that in HB.

**Acknowledgments** Thanks for International Science Editing to edit this paper. This project was supported by the National Natural Science Foundation of China (Contract No: 20801017, 20771033, 20973053, 21073051), the Natural Science Foundation of Hebei Province (Contract No: B2008000138, B2010000371), and the Education Department Foundation of Hebei Province (Contract No: 2007123, ZD2010126).

## References

1. Jeffrey GA (1997) An introduction to hydrogen bonding. Oxford University Press, Oxford
2. Shigorin DN (1959) Spectrochim Acta 14:169–179
3. Kollman PA, Liebman JF, Allen LC (1970) J Am Chem Soc 92:1142–1150
4. Ault BS, Pimentel GC (1975) J Phys Chem 79:621–626
5. Ammal SSC, Venuvanalingam P (1998) J Chem Phys 109:9820–9830
6. Ammal SSC, Venuvanalingam P (1997) J Chem Phys 107:4329–4336
7. Ott H, Däschlein C, Leusser D, Schildbach D, Seibel T, Stalke D, Strohmann C (2008) J Am Chem Soc 130:11901–11911
8. Sannigrahi AB, Kar T, Niyogi BG (1986) Proc Indian Acad Sci Chem Sci 96:253–258
9. Sannigrahi AB, Kar T, Niyogi BG, Hobza P (1990) Schleyer PvR. Chem Rev 90:1061–1076
10. Sapse AM, PvR S (eds) (1995) Lithium chemistry, theoretical and experimental overview. Wiley, New York
11. Vila A, Vila E, Mosquera RA (2006) Chem Phys 326:401–408
12. Ammal SSC, Venuvanalingam P, Paul S (2000) J Chem Phys 104:10859–10864
13. Piacenza M, Grimme S (2005) Chem Phys Chem 6:1554–1558
14. Caffarel M, Scemama A, Ramírez-Solís A (2010) Theor Chem Acc 126:275–287
15. Kim KS, Tarakeshwar PJ, Lee Y (2000) Chem Rev 100:4145–4185
16. Carcabal P, Seurre N, Chevalier M, Broquier M, Brenner V (2002) J Chem Phys 117:1522–1528
17. Foster RS (1969) Organic Charge Transfer Complexes. Academic, New York
18. Loudon GM (1988) Organic Chemistry, 2nd edn. Benjamin Cummings, Menlo Park
19. Legon AC, Millen DJ (1987) Chem Soc Rev 16:467–498
20. Legon AC (1999) Angew Chem Int Ed 38:2686–2714
21. Lesarri A, López JC, Alonso JL (1998) J Chem Soc Faraday Trans 94:729–733
22. Shea JA, Kukolich SG (1983) J Chem Phys 78:3545–3551
23. Cole GC, Legon AC, Ottaviani P (2002) J Chem Phys 117:2790–2799
24. Cooke SA, Corlett GK, Legon AC (1998) Chem Phys Lett 291:269–276
25. Cooke SA, Corlett GK, Legon AC (1998) J Chem Soc Faraday Trans 94:1565–1570
26. Cooke SA, Corlett GK, Holloway JH, Legon AC (1998) J Chem Soc Faraday Trans 94:2675–2680
27. Cooke SA, Holloway JH, Legon AC (1998) Chem Phys Lett 298:151–160
28. Wu JY, Zhang JC, Wang ZX, Cao WL (2007) J Chem Phys 127 (175102):1–7
29. Wang ZX, Zhang JC, Wu JY, Cao WL (2007) J Chem Phys 126 (134301):1–7
30. Frisch MJ, Trucks GW et al. (2004) Gaussian 03, Revision D.01. Gaussian Inc, Wallingford, CT
31. Boys SF, Bernardi F (1970) Mol Phys 19:553–566
32. Reed AE, Curtiss LA, Weinhold F (1988) Chem Rev 88:899–926
33. Politzer P, Murray JS, Clark T (2010) Phys Chem Chem Phys 12:7748–7757
34. Murray JS, Riley KE, Politzer P, Clark T (2010) Aust J Chem 63:1598–1607
35. Bader RFW (1990) Atoms in Molecules-A Quantum Theory. Oxford University Press, Oxford
36. Popelier P (2000) Atoms in Molecules: An Introduction. UMIST, Manchester
37. Matta CF, Boyd RJ (eds) (2007) The quantum theory of atoms in molecules. From solid state to DNA and drug design. Wiley-VCH, Weinheim
38. Biegler-König F (2000) AIM 2000, Version 1.0. University of Applied Science, Bielefeld, Germany
39. Zheng SJ, Cai XH, Meng LP (1995) QCPE Bull 15:25–28
40. Jabłoński M, Palusiak M (2010) J Phys Chem A 114:2240–2244
41. Li Y, Wu D, Li ZR, Chen W, Sun CC (2006) J Chem Phys 125 (084317):1–7
42. Feng Y, Liu L, Wang JT, Li XS, Guo QX (2004) Chem Commun 88-89
43. Li QZ, Wang HZ, Liu ZB, Li WZ, Cheng JB, Gong BA, Sun JZ (2009) J Phys Chem A 113:14156–14160
44. Li QZ, Wang YF, Li WZ, Cheng JB, Gong BA, Sun JZ (2009) Phys Chem Chem Phys 11:2402–2407
45. Yuan K, Zhu YC, Liu YZ, Li ZF, Dong XN, Wang XF, Li HX, Zhang J (2008) Chin Sci Bull 53:3151–3158
46. Bader RFW (2010) J Phys Chem A 114:7431–7444
47. Bohórquez HJ, Matta CF, Boyd RJ (2010) Int J Quantum Chem 110:2418–2425
48. Biswal HS, Shirhatti PR, Wategaonkar S (2010) J Phys Chem A 114:6944–6955
49. Yau AD, Byrd EFC, Rice BM (2009) J Phys Chem A 113:6166–6171
50. Grabowski SJ, Krygowski TM, Leszczynski J (2009) J Phys Chem A 113:1105–1110
51. Vener MV, Egorova AN, Fomin DP, Tsirelson VG (2007) Chem Phys Lett 440:279–285
52. Mohan N, Vijayalakshmi KP, Koga N, Suresh CH (2010) J Comput Chem 31:2874–2882
53. Dubis AT, Grabowski SJ (2002) New J Chem 26:165–169
54. Zeng YL, Meng LP, Li XY, Zheng SJ (2007) J Phys Chem A 111:9093–9101
55. Li XY, Fan HM, Meng LP, Zeng YL, Zheng SJ (2007) J Phys Chem A 111:2343–2350
56. Zeng YL, Zheng SJ, Meng LP (2004) Inorg Chem 43:5311–5320
57. Zheng SJ, Meng LP, Cai XH, Xu ZF, Fu XY (1997) J Comput Chem 18:1167–1174
58. Berski S, Latajka Z (2002) Int J Quantum Chem 90:1108–1120
59. Tang TH, Deretey E, Jensen SJK, Csizmadia IG (2006) Eur Phys J D 37:217–222
60. Cremer D, Kraka E (1984) Angew Chem Int Ed Engl 23:627–628
61. Bone RGA, Bader RFW (1996) J Phys Chem 100:10892–10911
62. Rozas I, Alkorta I, Elguero J (2000) J Am Chem Soc 122:11154–11161